2019 18th European Control Conference (ECC)
Napoli, Italy, June 25-28, 2019

# Exploring the dependence of cell aging dynamics on thermal gradient in battery modules: A PDE-based time scale separation approach

Anirudh Allam and Simona Onori

*Abstract*— **There is an abundance of research dedicated to understanding lithium-ion batteries at the cell-level. However, the cell-level models or estimation algorithms cannot be directly applied to battery modules or packs that are composed of tens to hundreds or thousands of cells. Pack or module-level modeling and estimation must take into consideration the temperature distribution, manufacturing-induced parameter (impedance, capacity) variances, pack topology (electrical interconnections), and thermal interactions between cells. In this work, we motivate the need for pack or module-level modeling by showing that the aging dynamics of a cell is influenced by the adjacent cells it is interacting with, both, electrically and thermally. The characteristic time-scale of the vital dynamics of an interconnected cell, consisting of a high-fidelity coupled electrochemical-thermal-aging model, are studied to reveal a three-time scale behavior. This distinct behavior is explored via singular perturbation theory to derive a reduced-order aging model for an interconnected cell that is shown to depend on the thermal gradient in a serially interconnected module.**

## I. INTRODUCTION

Large-scale systems composed of numerous individual components tend to lose modularity, wherein, the behavior of the entire system cannot be predicted based solely on the behavior of a constituting individual component [1]. Further, with the inclusion of faults or aging in the individual components, the complexity in predicting the behavior of the system increases. High energy density battery packs used in HEVs and EVs are large-scale complex interconnected systems made up of numerous individual cells interconnected to each other to satisfy the desired power and energy requirements. Modularity is assumed in the case of large-scale interconnected battery packs, in the sense that the behavior of the battery pack is extrapolated based on the behavior of an individual cell. This approach assumes homogeneity between cells, in terms of parameters, temperature and aging characteristics. However, instances reported in the literature suggest that modularity cannot be guaranteed in battery modules or packs. In summary,

1) Cell-to-cell manufacturing variances have a diverse effect on the aging characteristics of cells, and by extension will effect the overall behavior of the pack [2],
2) Thermal gradient experienced by a battery module or pack alters the aging trends of each cell, and hence the pack's health is limited by the most aged cell [3],
3) Inhomogeneity in aging characteristics between cells will create a thermal gradient in the module/pack [4], and
4) Battery pack ages faster than an individual cell subjected to the same operating conditions [5].

From the literature surveyed, it is understood that in battery modules/packs, initial manufacturing variances, uneven temperature distribution, differences in the aging characteristics of cells will cause aging at dissimilar rates in each cell due to the interconnected nature of a battery pack. This motivates the need to develop comprehensive modeling tools to understand the dynamics at the module or pack-level, rather than at the cell-level.

To that end, this work intends to show that in an interconnected setting, the aging dynamics of a cell is interlinked to the thermal gradient in the module, which is implicitly dependent on the degradation of the neighboring cells it is thermally and electrically interacting with. The cell dynamics are separated based on fast and slow dynamics by identifying the characteristic time scale of the dynamics. Singular perturbation theory is utilized to derive a reduced-order aging model that reveals the dependence on the neighboring cells. Similar work, using singular perturbation theory, was proposed in [6], [7], [8]. However, the singular perturbation approach used in these papers was at the cell-level. Further, a comprehensive way of discerning the characteristic time scales of the cell dynamics was missing.

The remainder of this article is organized as follows: Section II-A details the Doyle-Fuller-Newman (DFN) battery model, thermal and aging model. Section II-B describes a thermal model for a cell in a module by incorporating the heat transfer between its neighboring cells. Section III quantifies the characteristic time scale of the electrochemical, thermal, and aging Partial differential equations (PDEs) to formulate a three-time scale singular perturbation problem. Section IV derives the reduced-order aging model for an interconnected cell, by approximating the fast and semi-slow dynamics, that implicitly depends on the degradation of the neighboring cells. Finally, Section VI summarizes the conclusions and proposes future research direction.

## II. MODELING

The modeling section is divided into two parts. The first part describes the cell-level dynamics of a lithium-ion cell. The second part presents the modeling equation required to describe the thermal interaction between cells in a module.

The authors are with the Department of Energy Resources Engineering, Stanford University, Stanford, CA 94305, USA (aallam, sonori)@stanford.edu. S. Onori is the corresponding author.

### A. Cell Governing Equations

In this work, a lithium-ion cell model is described by a coupled electrochemical-thermal-aging model. The DFN model, also known as the Pseudo two-dimensional (P2D) model, is used to represent the nonlinear transport mechanisms in the solid and electrolyte phase of the battery through a system of partial differential algebraic equations. The governing electrochemical dynamics are tabulated in Table I. The thermal model, given in (9) in Table I, describes the radially varying temperature profile via a one-dimensional cylindrical heat PDE. The thermal model assumes that the surface temperature remains uniform throughout the surface and the heat is uniformly generated in radial direction. Next, a diffusion-limited aging model, described by (10) to (14) in Table I, representing the growth of Solid Electrolyte Interphase (SEI) layer on the anode is considered. Further, the empirical relationship of the Open Circuit Potential with respect to the solid surface concentration and the temperature-dependency of transport parameters are borrowed from the literature [9].

### B. Module Governing Equations

The governing equations in Table I describe the cell-level dynamics, however, it is important to incorporate the modifications brought about by connecting the cell to a network of other cells. Cells packed closely together in a module thermally interact with each other [7], [3]. The heat transfer through conduction between the surface of neighboring cells must be incorporated while modeling a module or pack-level interconnected cell network. This conductive heat transfer is accommodated into the boundary condition of the thermal PDE given in (9). The general equation describing the radial temperature profile remains the same, but a modified boundary condition taking into account the effect of heat transfer between cells is included. Here, a thermal model of a cell $i$, connected in series with cells $i-1$ and $i+1$, as shown in Fig. 1, is given by

$$\frac{1}{\alpha}\frac{\partial T_i}{\partial t} = \frac{\partial^2 T_i}{\partial r_c^2} + \frac{1}{r_c}\frac{\partial T_i}{\partial r_c} + \frac{Q_i}{k_{cell}}, \tag{15}$$

with the following Neumann boundary conditions

$$\begin{aligned} \frac{\partial T_i}{\partial r_c}\Big|_{r_c=0} &= 0 \\ \frac{\partial T_i}{\partial r_c}\Big|_{r_c=R_c} &= -\frac{hA_{cell}}{k_{cell}}\left(T_i - T_{amb}\right) - \frac{h_m A_{cell}}{2k_{cell}}\left(T_i - T_{i-1}\right) \\ &\quad - \frac{h_m A_{cell}}{2k_{cell}}\left(T_i - T_{i+1}\right), \end{aligned} \tag{16}$$

where $h_m$ is the heat transfer coefficient between cells in a module.

## III. TIME SCALE ANALYSIS

It is understood that the cell dynamics evolve at multiple time scales [6], [7], [8]. However, the attempts at showing this multi-time scale behavior have been preliminary [6], [7] or via simulation [8]. Instead, in this paper, a formal method for examining the multi-time scale behavior of cell dynamics is investigated. The dynamics under study are the

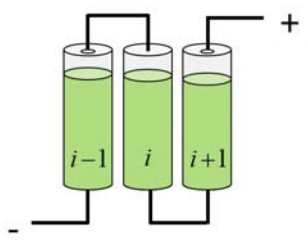


Fig. 1. A representation of the simulated battery module with three cells $i-1$, $i$, and $i+1$ connected in series.

electrochemcial, thermal, and aging dynamics described by their respective PDEs in (1), (15), and (10), respectively. The respective PDEs are non-dimensionalized and their characteristic time scales are extracted in terms of actual physical transport parameters. The benefit of identifying the multi-time scale behavior is to make use of singular perturbation theory to help derive a reduced order model. By obtaining a reduced order model, the faster dynamics need not be solved numerically, instead its approximate quasi-steady state solutions can be used to solve the "slow" model that approximates the system behavior reasonably well. To that end, the identification of time scales is used to formulate the battery dynamics into a standard singular perturbation format.

Consider the PDEs in (1), (15), and (10). Normalizing the respective PDEs with respect to their length scale by introducing the following non-dimensional parameters

$$\bar{r} = \frac{r}{R_n} \qquad \bar{r}_c = \frac{r_c}{R_{cell}}, \tag{17}$$

gives the following PDEs

$$\begin{cases} \dfrac{\partial T_i}{\partial t} &= \dfrac{\alpha}{R_c^2}\dfrac{\partial^2 T_i}{\partial \bar{r}_c^2} + \dfrac{\alpha}{R_c^2 \bar{r}_c}\dfrac{\partial T_i}{\partial \bar{r}_c} + \dfrac{\alpha Q_i}{k_{cell}} \\ \dfrac{\partial c_{s,n}}{\partial t} &= \dfrac{D_{s,n}}{R_n^2 \bar{r}^2}\dfrac{\partial}{\partial \bar{r}}\left[\bar{r}^2 \dfrac{\partial c_{s,n}}{\partial \bar{r}}\right] \\ \dfrac{\partial c_{solv}}{\partial t} &= \dfrac{D_{solv}}{R_n^2}\dfrac{\partial^2 c_{solv}}{\partial \bar{r}^2} - \dfrac{1}{R_n}\dfrac{dL_{sei}}{dt}\dfrac{\partial c_{solv}}{\partial \bar{r}}. \end{cases}$$

Selecting a time scale given by $\tau = \dfrac{t}{t_{sei}}$, where $t_{sei}$ is the characteristic time scale of the aging dynamics, and substituting into the above equations gives

$$\begin{cases} \dfrac{1}{t_{sei}}\dfrac{\partial T_i}{\partial \tau} &= \dfrac{\alpha}{R_c^2}\dfrac{\partial^2 T_i}{\partial \bar{r}_c^2} + \dfrac{\alpha}{R_c^2 \bar{r}_c}\dfrac{\partial T_i}{\partial \bar{r}_c} + \dfrac{\alpha Q_i}{k_{cell}} \\ \dfrac{1}{t_{sei}}\dfrac{\partial c_{s,n}}{\partial \tau} &= \dfrac{D_{s,n}}{R_n^2 \bar{r}^2}\dfrac{\partial}{\partial \bar{r}}\left[\bar{r}^2 \dfrac{\partial c_{s,n}}{\partial \bar{r}}\right] \\ \dfrac{1}{t_{sei}}\dfrac{\partial c_{solv}}{\partial \tau} &= \dfrac{D_{solv}}{R_n^2}\dfrac{\partial^2 c_{solv}}{\partial \bar{r}^2} - \dfrac{1}{R_n t_{sei}}\dfrac{dL_{sei}}{d\tau}\dfrac{\partial c_{solv}}{\partial \bar{r}}. \end{cases}$$

Indicating the characteristic time scale of the electrochemical and thermal dynamics as $t_c$ and $t_\theta$, respectively, and defining the characteristic time scales for each PDE as follows

$$t_c = \frac{R_n^2}{D_{s,n}}, \quad t_\theta = \frac{R_c^2}{\alpha}, \quad t_{sei} = \frac{R_n^2}{D_{solv}}, \tag{18}$$

TABLE I

ELECTROCHEMICAL-THERMAL-AGING DYNAMICS OF A LITHIUM-ION CELL

| | | |
|---|---|---|
| **Electrochemical dynamics [10], [11]** | | |
| Mass conservation in solid phase | $\frac{\partial c_{s,j}}{\partial t} = \frac{D_{s,j}}{r^2}\frac{\partial}{\partial r}\left[r^2\frac{\partial c_{s,j}}{\partial r}\right]$ <br> $\frac{\partial c_{s,j}}{\partial r}\Big\vert_{r=0} = 0 \quad \frac{\partial c_{s,j}}{\partial r}\Big\vert_{r=R_j} = \frac{-i_{int,j}}{D_{s,j}a_{s,j}F}$ | (1) |
| Mass conservation in electrolyte phase | $\epsilon_e\frac{\partial c_e}{\partial t} = \frac{\partial}{\partial x}\left(D_e^{eff}\frac{\partial c_e}{\partial x}\right) + \left(1-t_0^+\right)\frac{\pm i_{int,j}}{F}$ <br> $\frac{\partial c_e}{\partial l}\Big\vert_{l=0} = \frac{\partial c_e}{\partial l}\Big\vert_{l=L} = 0$ <br> $D_{e,n}^{eff}(c_{e,n},T)\left(\frac{\partial c_{e,n}}{\partial l}(l,t)\right)\Big\vert_{l=L_n} = D_{e,s}^{eff}(c_{e,s},T)\left(\frac{\partial c_{e,s}}{\partial l}(l,t)\right)\Big\vert_{l=L_n}$ <br> $D_{e,s}^{eff}(c_{e,s},T)\left(\frac{\partial c_{e,s}}{\partial l}(l,t)\right)\Big\vert_{l=L_n+L_s} = D_{e,p}^{eff}(c_{e,p},T)\left(\frac{\partial c_{e,s}}{\partial l}(l,t)\right)\Big\vert_{l=L_n+L_s}$ | (2) |
| Charge conservation in solid phase | $\frac{\partial}{\partial x}\left(\sigma_{eff}\frac{\partial \Phi_s}{\partial x}\right) - a_{s,j}i_{int,j} = 0$ | (3) |
| | $\frac{\partial \Phi_s}{\partial x}\Big\vert_{x=L_n} = \frac{\partial \Phi_s}{\partial x}\Big\vert_{x=L_n+L_s} = 0$ | (4) |
| | $\frac{\partial \Phi_s}{\partial x}\Big\vert_{x=L_n+L_s+L_p} = I_{batt}$ | (5) |
| Charge conservation in electrolyte phase | $\kappa^{eff}\frac{\partial^2\phi_e}{\partial x^2} - \kappa_D^{eff}\frac{\partial^2 \ln c_e}{\partial x^2} + a_{s,j}i_{int,j} = 0$ <br> $\frac{\partial \Phi_e}{\partial x}\Big\vert_{x=0} = \frac{\partial \Phi_e}{\partial x}\Big\vert_{x=L_n+L_s+L_p} = 0$ | (6) |
| Intercalation current | $i_{int,j} = a_{s,j}i_{0,j}\left[\exp\left(\frac{F\eta_j}{2R_gT}\right) - \exp\left(\frac{-F\eta_j}{2R_gT}\right)\right]$ | (7) |
| Cell voltage | $V = \Phi_s\Big\vert_{x=L_n+L_s+L_p} - \Phi_s\Big\vert_{x=0} - I_{batt}R_l$ | (8) |
| **Thermal dynamics [12]** | | |
| Heat balance | $\frac{1}{\alpha}\frac{\partial T}{\partial t} = \frac{\partial^2 T}{\partial r_c^2} + \frac{1}{r_c}\frac{\partial T}{\partial r_c} + \frac{Q_{cell}}{k_{cell}}$ <br> $\frac{\partial T}{\partial r_c}\Big\vert_{r_c=0} = 0 \quad \frac{\partial T}{\partial r_c}\Big\vert_{r_c=R_c} = -\frac{hA_{cell}}{k_{cell}}(T-T_{amb})$ | (9) |
| **Aging dynamics [13], [14], [15]** | | |
| Mass conservation in SEI | $\frac{\partial c_{solv}}{\partial t} = D_{solv}\frac{\partial^2 c_{solv}}{\partial r^2} - \frac{dL_{sei}}{dt}\frac{\partial c_{solv}}{\partial r}$, | (10) |
| | $-D_{solv}\frac{\partial c_{solv}}{\partial r}\Big\vert_{r=Rn} + \frac{dL_{sei}}{dt}c_{solv}^* = \frac{i_s}{F}$ | (11) |
| SEI layer growth | $\frac{dL_{sei}}{dt} = -\frac{i_s M_{sei}}{2F\rho_{sei}}$, | (12) |
| Side reaction current density | $i_s = 2Fk_f c_{surf,n}^2 c_{solv}\exp\left[\frac{-\beta F}{RT_c}\left(\Phi_{s,n} - \frac{L_{sei}I_{batt}}{\kappa_{sei}}\right)\right]$ | (13) |
| Cell capacity loss | $\frac{dQ}{dt} = i_s A L_n a_{s,n}$ | (14) |

and assigning values to the ratio of the characteristic time scales as

$$\lambda_1 = \frac{t_c}{t_{sei}}, \quad \lambda_2 = \frac{t_\theta}{t_c}, \quad \lambda_1\lambda_2 = \frac{t_\theta}{t_{sei}}, \tag{19}$$

where $\lambda_1, \lambda_2$ are constant parameters that are obtained by plugging values from the literature, leads to the following inequality holding true: $0 < \lambda_1\lambda_2 < \lambda_1 < 1$. Substituting the characteristic time scale of each PDE and then rewriting in terms of $\lambda_1$ and $\lambda_2$ puts the dynamics in a standard three-time scale singular perturbation format as follows

$$\begin{cases} \lambda_1\lambda_2\dfrac{\partial T_i}{\partial \tau} = & \dfrac{\partial^2 T_i}{\partial \bar{r}_c^2} + \dfrac{1}{\bar{r}_c}\dfrac{\partial T_i}{\partial \bar{r}_c} + \dfrac{R_c^2 Q_i}{k_{cell}} \\ \lambda_1\dfrac{\partial c_{s,n}}{\partial \tau} = & \dfrac{1}{\bar{r}^2}\dfrac{\partial}{\partial \bar{r}}\left[\bar{r}^2\dfrac{\partial c_{s,n}}{\partial \bar{r}}\right] \\ \dfrac{\partial c_{solv}}{\partial \tau} = & \dfrac{\partial^2 c_{solv}}{\partial \bar{r}^2} - \dfrac{1}{R_n}\dfrac{dL_{sei}}{d\tau}\dfrac{\partial c_{solv}}{\partial \bar{r}}. \end{cases} \tag{20}$$

In the above formulation, the thermal dynamics are considered to be the fast dynamics, the concentration PDE is the semi-slow dynamics, and the aging PDE represents the slow dynamics, which is based on the values obtained for $\lambda_1$ and $\lambda_2$.

## IV. REDUCED ORDER MODEL

In the context of understanding the effect of thermal gradient on the aging dynamics of an interconnected cell, the three time scale behavior described in (20) is exploited via singular perturbation theory to derive a 'slow' reduced order aging model where the fast and semi-slow dynamics are approximated by their quasi steady state values.

The procedure to obtain the quasi steady-state solutions for the fast and semi-slow dynamics is straight forward, however, the theoretical work involved in deriving the solution is involved and hence omitted from this manuscript. The detailed theoretical proof work will feature in a forthcoming paper. For the thermal dynamics, the procedure involves setting $\lambda_1\lambda_2 = 0$ to obtain a quasi steady state solution at the cell's core (core temperature). The solution will be dependent on the heat transfer between the cell and the environment,

TABLE II
NOMENCLATURE

| | | | | | |
|---|---|---|---|---|---|
| $A$ | Cell cross sectional area [$m^2$] | $D_e$ | Electrolyte phase diffusion [$m^2$/s] | $D_e^{eff}$ | Effective electrolyte phase diffusion [$m^2$/s] |
| $D_{s,j}$ | Solid phase diffusion [$m^2$/s] | $D_{solv}$ | Solvent diffusion in SEI layer [$m^2$/s] | $c_{solv}$ | Solvent concentration at the surface [mol/$m^3$] |
| $F$ | Faraday's constant [C/mol] | $L_j$ | Domain thickness [m] | $L_{sei}$ | SEI layer thickness [m] |
| $M_{sei}$ | Molar mass of SEI layer [kg/mol] | $R_g$ | Universal gas constant [J/mol-K] | $R_j$ | Particle radius [m] |
| $R_l$ | Lumped resistance [$\Omega$] | $R_{sei}$ | SEI layer resistance [$\Omega$] | $T$ | Cell temperature [$^o$C] |
| $\alpha$ | Thermal diffusivity | $U_j$ | Open circuit potential [V] | $V$ | Cell terminal voltage [V] |
| $a_{s,j}$ | Specific interfacial surface area [$m^{-1}$] | $c_e$ | Concentration in liquid phase [mol/$m^3$] | $R_c$ | Radius of a cylindrical 18650 cell [m] |
| $c_{s,j}$ | Concentration in solid phase [mol/$m^3$] | $A_{cell}$ | External cell surface area [$m^2$] | $c_{s,j,surf}$ | Concentration at the surface [mol/$m^3$] |
| $c_{s,j,max}$ | Maximum electrode concentration [mol/$m^3$] | $i_s$ | Side reaction current density [A/$m^2$] | $k_j$ | Reaction rate constant [$m^{2.5}$/s-$mol^{0.5}$] |
| $x$ | Cartesian coordinate along the cell's thickness | $r$ | Radial coordinate | $t_0^+$ | Transference number |
| $\Phi_j$ | Potential [V] | $\epsilon_j$ | Active volume fraction of solid phase | $\epsilon_{e,j}$ | Porosity |
| $\epsilon_{j,f}$ | Active volume fraction of filler/binder | $\kappa$ | Electrolyte conductivity [S/m ] | $\kappa_{sei}$ | SEI layer ionic conductivity [S/m] |
| $\kappa^{eff}$ | Effective electrolyte conductivity [S/m] | $\eta_j$ | Overpotential [V] | $k_{cell}$ | Thermal conductivity |
| $T_c$ | Core Temperature [$^o$C] | $r$ | Radial co-ordinate for active particle | $r_c$ | Radial co-ordinate for 18650 cell |
| $h$ | Heat transfer co-efficent | $\rho_{sei}$ | SEI layer density [kg/$m^3$] | Subscript $j$ | Refers to anode, separator, or cathode |

the internal heat generated, and the heat transfer between the cell and its neighboring cells, which enters the steady state equation through the Neumann boundary condition at the surface of the cell. For the electrochemical dynamics, setting $\lambda_1 = 0$ and applying the theory of averaging [16] gives the quasi steady state solution, which will be used in the slow reduced-order model. For ease of explanation, we denote the quasi-steady state values of core temperature and concentration dynamics of cell $i$ as $\bar{T}_{c,i}$ and $\bar{c}_{s,n}$. Note that the quasi steady state solutions can be written in general form as

$$\begin{cases} \bar{T}_i = & f\left(\bar{T}_i, \bar{T}_{i-1}, \bar{T}_{i+1}, T_{amb}, I_{batt}\right) \\ \bar{c}_{s,n} = & g\left(\bar{c}_{s,n}, \bar{T}_i, I_{batt}\right) \end{cases} \tag{21}$$

This leads to the following aging model equations, which we refer to as the reduced-order model.

$$\begin{cases} \dfrac{\partial c_{solv}}{\partial \tau} & = \dfrac{\partial^2 c_{solv}}{\partial \bar{r}^2} - \dfrac{1}{R_n}\dfrac{dL_{sei}}{d\tau}\dfrac{\partial c_{solv}}{\partial \bar{r}}. \\ \dfrac{dL_{sei}}{d\tau} & = -\dfrac{i_s M_{sei} t_{sei}}{2F\rho_{sei}} \\ i_s & = 2Fk_f \bar{c}_{surf,n}^2 c_{solv} \\ & \quad \exp\left[\dfrac{-\beta F}{R\bar{T}_{c,i}}\left(\Phi_{s,n} - \dfrac{L_{sei} I_{batt}}{\kappa_{sei}}\right)\right] \end{cases} \tag{22}$$

The quasi steady-state solution for the fast and semi-slow dynamics embedded within the side reaction current density $i_{s,i}$ equation enters the aging PDE through its boundary condition. It is evident that the aging dynamics are now dependent on the temperature difference between cells or the thermal inhomogeneity between cells. This model can be used to quantify the effect thermal gradient on the aging dynamics of a particular interconnected cell. Further, in future work, this model will be used to develop strategies that can be used to attenuate the effect of thermal gradient on aging dynamics of an interconnected cell, through efficient thermal control or cell balancing control.

## V. RESULTS

### A. Experimental Results

The experimental setup consists of Arbin BT2000 battery testing system, environmental chamber, and peltier junctions for temperature controlled cell testing, and current and voltage data acquisition. Cylindrical Nickel Manganese Cobalt (NMC) lithium-ion cells of 2Ah capacity are subjected to predetermined input current profiles and the resulting cell voltage is logged for the model identification procedure.

The DFN battery model parameters are identified experimentally by minimizing the error between the model voltage and the measured voltage data. A global optimization algorithm (particle swarm) is utilized to identify the DFN model parameters. For the identification procedure, a 2A (1C-rate) constant discharge current profile is used. The identified model's voltage response is compared against the experimentally measured cell voltage as shown in Fig. 2. To validate the performance of the identified battery model against a different current profile, a real-world US06 drive cycle is used. The current profile is generated for a hybrid electric vehicle and scaled for a single cell. The input current profile and the voltage comparison result is presented in Fig. 3. The RMS voltage error between the model and measured voltage is as low as 9.2mV.

### B. Simulation Results

A module of three cells connected in series is considered for the simulation studies, as shown in Fig. 1. The electrochemical dynamics of each cell in the module is described by the experimentally validated DFN model in Section V-A. Each cell also contains a thermal and aging model, described

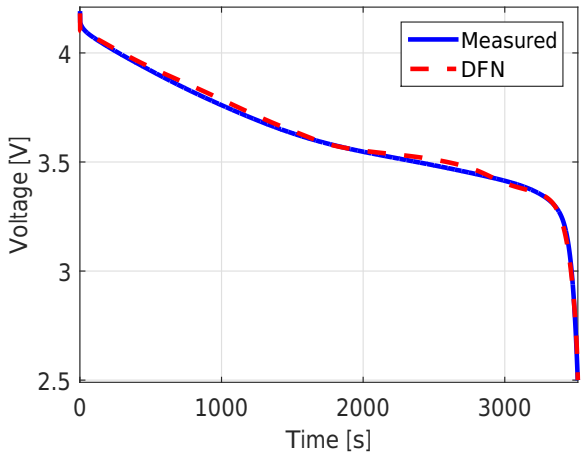


Fig. 2. Voltage comparison between measured data and DFN (simulated).

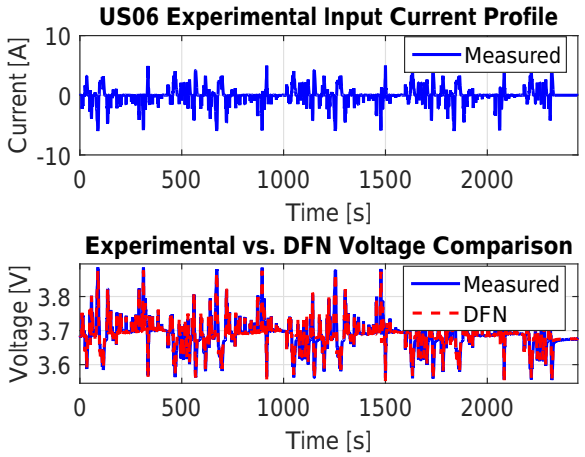


Fig. 3. DFN model validation against experimental data for the US06 current profile.

in Section II-A, whose parameters are borrowed from the literature. The thermal interactions between the cells in the module is described by the model in Section II-B. Together, this constitutes a high-fidelity model of a battery module with three cells in series. This model is considered to be the baseline model, and shall be used in validating the reduced-order aging model derived via singular perturbation theory. Upon satisfactory validation, the reduced-order aging model will be used to understand the effect of a thermal gradient on the aging of cells in an interconnected framework.

*1) Reduced-order model validation:* Prior to making use of the reduced-order aging model it must be validated against the full order model. For this case, a simulation current profile containing a train of discharge and charge currents is cycled for 30 days, within a state of charge window of 30 - 80%. Also, there is no thermal gradient induced in the module, meaning that all cells are starting at the same temperature of $30^oC$, while the ambient temperature is set at $45^oC$. The growth of the SEI layer thickness of cell $i$ simulated via the model of the battery module is logged

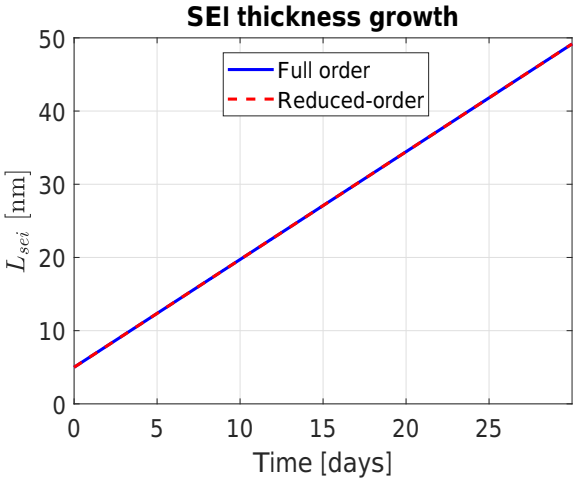


Fig. 4. Validation of full-order SEI layer growth model with the derived reduced-order SEI model.

and plotted in Fig. 4, indicated by Full-order in the legend. Whereas, the SEI layer thickness growth in the reduced-order model derived by substituting the quasi-steady state values of the fast and semi-slow variables, as given in (22) is plotted in Fig. 4. The derived model does not lose its accuracy when compared to the full-order model. However, it is worth noting that this may not be valid as the battery ages or under different operating conditions and current profiles. A detailed study understanding the validity and limitations of using this reduced-order model will be investigated in the future.

*2) Effect of thermal gradient on aging of interconnected cell:* Having shown that the reduced-order aging model is capable of predicting the SEI layer growth accurately, under the specified operating conditions, we intend use this low complexity model to investigate the effect of gradients (thermal, aging, or cell-to-cell parameter variances) on the aging dynamics of cells in an interconnected module. In this work, we limit our study to show that a thermal gradient in a module, will cause increased rate of growth of the SEI layer in cells, and hence, higher capacity loss, which would eventually lead to a faster overall aging of the pack.

To that end, a conservative thermal gradient is induced manually, such that the cell $i-1$ operates at a temperature of $0.8^oC$ higher than cell $i$, and the cell $i+1$ operates at a temperature of $1^oC$ higher than cell $i$. The input current and ambient temperature conditions are maintained the same as the simulation in Section V-B.1.

The SEI layer thickness growth of cell $i$ in the absence of a thermal gradient is denoted as Case 1. The SEI layer thickness growth of cell $i$ in the presence of a thermal gradient is denoted as Case 2. The comparison of the SEI layer growth for both cases, as shown in Fig. 5, indicates the effect of thermal gradient on the increase in the rate of growth of the SEI layer in cell $i$. The SEI layer growth is translated into tangible terms, such as capacity loss, and plotted in Fig. 6. The same trend is noticed in the capacity loss plot, showing that the capacity of cell $i$ fades faster when

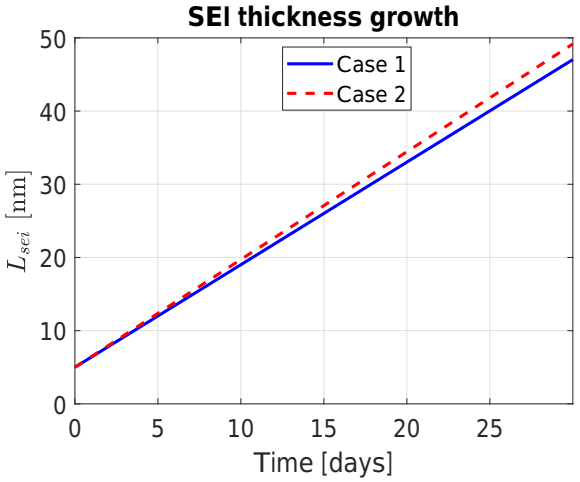


Fig. 5. Comparison of SEI layer thickness growth of cell $i$ (connected in series with cells $i-1$ and $i+1$) for the case with no thermal gradient in a module (Case 1) and with a thermal gradient (Case 2).

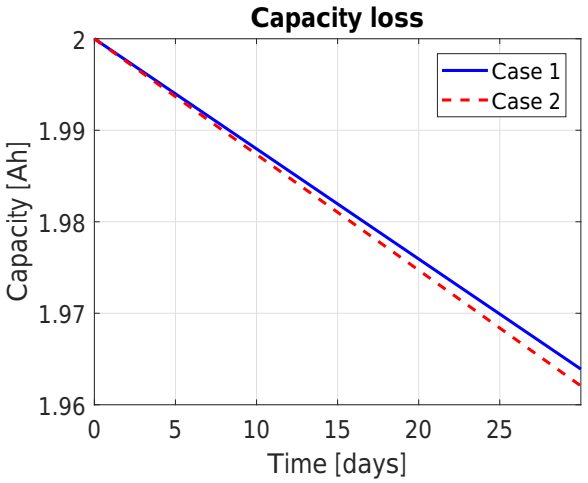


Fig. 6. Comparison of capacity of cell $i$ (connected in series with cells $i-1$ and $i+1$) for the case with no thermal gradient in a module (Case 1) and with a thermal gradient (Case 2). A capacity loss of $0.09\%$ is observed due to the thermal gradient.

the module has a thermal gradient, as opposed to when there is no thermal gradient. A capacity loss of $0.09\%$ is observed due to the induced thermal gradient. Note that the thermal gradient is low in value and the simulation time period is short. As the battery ages, the capacity loss of cell $i$ in Case 2 will deviate further away from the Case 1, making the pack age faster.

## VI. CONCLUSION

This paper addresses the issue of understanding the effect on aging dynamics of a cell in a module due to a thermal gradient. To that end, a high-fidelity battery module is developed for simulations, consisting of a DFN model describing the electrochemical dynamics, a thermal model, and a diffusion-limited SEI layer aging model. In addition, the thermal interactions between cells in a module are incorporated. The three-time scale behavior in battery dynamics is characterized based on PDE-based time-scale analysis. This behavior is used to derive a reduced-order aging model for an interconnected cell in a module via singular perturbation theory, which is validated against a full-order model of a cell in a battery module. Further, the effect in the rate of SEI layer growth or capacity fade is presented in the presence of a thermal gradient in the module, thereby motivating the need for detailed study of the dependence of aging dynamics on battery module-based gradients.

Future work includes utilizing the reduced-order aging model to develop detailed understanding of the effect of cell-to-cell manufacturing variances, aging gradients, electrical topology, on the aging dynamics of a cell in a module.

## REFERENCES


[1] D. Del Vecchio, E. D. Sontag, and A. J. Ninfa, "Modular cell biology: retroactivity and insulation," *Molecular Systems Biology*, vol. 4, no. 1, pp. 161–n/a, 2008.

[2] T. Baumhöfer, M. Brühl, S. Rothgang, and D. U. Sauer, "Production caused variation in capacity aging trend and correlation to initial cell performance," *Journal of Power Sources*, vol. 247, pp. 332–338, 2014.

[3] K.-C. Chiu, C.-H. Lin, S.-F. Yeh, Y.-H. Lin, C.-S. Huang, and K.-C. Chen, "Cycle life analysis of series connected lithium-ion batteries with temperature difference," *Journal of Power Sources*, vol. 263, pp. 75–84, 2014.

[4] R. Gogoana, M. B. Pinson, M. Z. Bazant, and S. E. Sarma, "Internal resistance matching for parallel-connected lithium-ion cells and impacts on battery pack cycle life," *Journal of Power Sources*, vol. 252, pp. 8–13, 2014.

[5] T. R. Tanim, M. G. Shirk, R. L. Bewley, E. J. Dufek, and B. Y. Liaw, "Fast charge implications: Pack and cell analysis and comparison," *Journal of Power Sources*, vol. 381, pp. 56–65, 2018.

[6] A. Allam, S. Onori, S. Marelli, and C. Taborelli, "Battery health management system for automotive applications: A retroactivity-based aging propagation study." Proceedings of the American Control Conference, 2015, pp. 703–716.

[7] A. Allam and S. Onori, "Characterization of aging propagation in lithium-ion cells based on an electrochemical model," in *American Control Conference (ACC), 2016*. American Automatic Control Council (AACC), 2016, pp. 3113–3118.

[8] C. Zou, C. Manzie, and D. Nešić, "A framework for simplification of pde-based lithium-ion battery models," *IEEE Transactions on Control Systems Technology*, vol. 24, no. 5, pp. 1594–1609, 2016.

[9] T. R. Tanim, C. D. Rahn, and C.-Y. Wang, "A temperature dependent, single particle, lithium ion cell model including electrolyte diffusion," *Journal of Dynamic Systems, Measurement, and Control*, vol. 137, no. 1, p. 011005, 2015.

[10] M. Doyle, T. F. Fuller, and J. Newman, "Modeling of galvanostatic charge and discharge of the lithium/polymer/insertion cell," *J. Electrochem. Soc.*, vol. 140, no. 6, pp. 1526–1533, 1993.

[11] E. Martínez-Rosas, R. Vasquez-Medrano, and A. Flores-Tlacuahuac, "Modeling and simulation of lithium-ion batteries," *Computers & Chemical Engineering*, vol. 35, no. 9, pp. 1937–1948, 2011.

[12] S. Al Hallaj, H. Maleki, J.-S. Hong, and J. R. Selman, "Thermal modeling and design considerations of lithium-ion batteries," *Journal of Power Sources*, vol. 83, no. 1-2, pp. 1–8, 1999.

[13] P. Ramadass, B. Haran, P. M. Gomadam, R. White, and B. N. Popov, "Development of First Principles Capacity Fade Model for Li-Ion Cells," *Journal of The Electrochemical Society*, vol. 151, no. 2, pp. A196–A203, 2004.

[14] M. Safari, M. Morcrette, A. Teyssot, and C. Delacourt, "Multimodal physics-based aging model for life prediction of li-ion batteries," *JOURNAL OF THE ELECTROCHEMICAL SOCIETY*, vol. 156, no. 3, pp. A145–A153, 2009.

[15] E. Prada, D. Di Domenico, Y. Creff, J. Bernard, V. Sauvant-Moynot, and F. Huet, "A Simplified Electrochemical and Thermal Aging Model of LiFePO4-Graphite Li-ion Batteries: Power and Capacity Fade Simulations," *Journal of The Electrochemical Society*, vol. 160, no. 4, pp. A616–A628, 2013.

[16] F. Verhulst, "On averaging methods for partial differential equations," *Symmetry and perturbation theory*, pp. 79–95, 1999.